



Investigation of coloration efficiency for tungsten oxide–silver nanocomposite thin films with different surface morphologies

Hamed Najafi-Ashtiani¹ · Ali Bahari² · Samira Gholipour²

Received: 1 November 2017 / Accepted: 6 January 2018 / Published online: 17 January 2018
© Springer Science+Business Media, LLC, part of Springer Nature 2018

Abstract

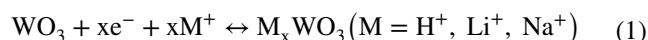
Tungsten oxide electrochromic (EC) thin films are prepared by physical vapor deposition (PVD) method in vacuum on fluorine doped tin oxide (FTO) coated glass substrate. In order to provide different surface morphology, the FTO-coated glass substrates are used in two different modes. The first sample is deposited at an angle of 0° and the second sample deposited at an angle of 75°. In this method, WO₃ nanoparticles powder with the same rate are deposited in vacuum. The Ag nanoparticles powder is utilized to decorate the surface of each of WO₃ thin films by using PVD method. The EC thin films are annealed to inject the Ag nanoparticles into the surface of thin films. The band gap of WO₃–Ag thin films are reported for indirect transitions. EC properties of WO₃–Ag thin films are investigated by cyclic voltammetry and the visible transmittance to compare the influence of surface morphology of WO₃–Ag thin films on EC performance. In particular, a significant optical modulation (40.59% at 632.8 nm) and high coloration efficiency (90.2 cm² C⁻¹ at 632.8 nm) are enhanced for the second sample compared to the first sample.

1 Introduction

In the last decades, most efforts to efficiently enhance energy efficiency have been focused on energy solution strategies utilizing the lithium ion batteries and super capacitors as energy storage systems and chromogenic materials in smart windows as efficient energy usage systems [1–4]. Not only energy storage systems are based on the electrochemical reaction of the electrode materials but also smart window systems are designed on the same mechanism and both of them possess sandwich device structures. Substantially designed energy-saving windows, such as electrochromic (EC), thermochromic and photochromic, function by exterior stimuli involving either an electric field, heat stimulus or ultraviolet (UV) excitation [5]. It is not possible to alter the optical performance, which involves arbitrarily passing or blocking solar energy in response to environmental changes in thermochromic and photochromic phenomena. While the important advantage of EC phenomenon that

can be exhibited is a controllable process independent from environmental changes [6, 7]. Balzers (in 1953) and Deb (in 1961) were the first researchers that were introduced a description of EC performance in transition metal oxides. This particular property is caused the attempts to use electrochromic devices (ECD) from 1953 to now [8]. This functionality is of great interest for numerous applications such as smart windows, switchable mirrors, information displays, sunglasses and variable emittance infrared skins [9–11].

Electrochromism is defined as reversible changes of the optical properties of materials under an applied electric field. During an EC process, the electrons are injected or extracted depending on applied voltage and the ions are moved simultaneously into or out of the EC materials to balance charge neutrality [12]. Recently more and more attention has been put on WO₃ thin films for its EC properties [13, 14]. The reversible EC effect in the case of WO₃ can be expressed as [15, 16]:



Furthermore, the nanocomposite structures of WO₃ containing metal nanoparticles have aroused great interest tremendous potential due to their unique chemical and physical properties. Nanoparticle of metals are manipulated to use unique optical properties that result mainly from its surface plasmon resonance (SPR) [17]. In EC

✉ Hamed Najafi-Ashtiani
h.najafi@velayat.ac.ir; hamednajafi59@yahoo.com

¹ Faculty of Basic Sciences, Department of Physics, Velayat University, Iranshahr, Iran

² Faculty of Basic Sciences, Department of Physics, University of Mazandaran, Babolsar, Iran

process, when the semiconductor such as WO_3 is coupled with a noble metal (Ag), electrons from the semiconductor transfer to the metal particles, as the Fermi energy level of the semiconductor is higher than that of the noble metal. Hence, the photo-generated electrons accumulate on the noble metal which serves as trap centers to facilitate charge separation [18].

In the present work, we use two modes to deposit the WO_3 thin films. Our purpose of different deposition modes is to provide the different surface morphologies of the samples. Because of, we use orientable substrate holder in deposition process by physical vapor deposition (PVD) apparatus. The angles of zero and 75° are adopted for substrate holder of samples. After deposition of WO_3 thin films at two modes, the WO_3 -Ag thin films are prepared by deposition of Ag nanoparticles on the surface of each samples. The EC properties of the WO_3 -Ag thin films are investigated by cyclic voltammetry (CV) and UV-Vis spectroscopy.

2 Experimental

2.1 Materials

WO_3 nanoparticles powder, Ag nanoparticles powder, lithium perchlorate, propylene carbonate (PC), deionized water (DI), ethanol and acetone are purchased from Merck. The fluorine doped tin oxide (FTO)-coated glass is purchased and cut into small pieces with the size of $0.9 \times 2.0 \text{ cm}^2$.

2.2 Instruments

Deposition of the thin films is done by PVD Apparatus (Meca 2000, France) that equipped with thickness gauge and operated in 10^{-6} torr. CV analyses are done by using the potentiostat/galvanostat Autolab (Nova software model PGSTAT 302N, Metrohm, Netherlands) coupled with a personal computer. CV is measured in 0.5 M LiClO_4 in PC solution that the FTO-coated glass slide is used as the working electrode and a thin foil of platinum and Ag/AgCl (KCl saturated) are used as counter and reference electrodes, respectively. The morphology of the thin film is characterized by a field emission scanning electron microscopy (FESEM, model MIRA3 TESCAN, operated at 15 kV) and an atomic force microscopy (AFM, model: Auto probe, cp-research, Veeco). Element identification results are obtained by energy disperse X-ray spectroscopy (EDX). The optical properties of the films are investigated by UV-Vis spectrophotometer (Shimadzu 210 spectrophotometer).

2.3 Preparation of WO_3 -Ag nanocomposite thin films

The WO_3 nanoparticles are deposited on the FTO-coated glass substrates (resistance $28\text{--}34 \ \Omega/\text{cm}^2$) using PVD method in vacuum at two different modes schematically illustrated in Fig. 1. Firstly, the FTO-coated glass is cleaned with common detergent and water, HCl 0.1 M, ethanol and finally acetone for 10 min in the ultrasonic bath and at room temperature, respectively. In the first state, FTO-coated glass substrate is placed at an angle of 0° corresponding to evaporation direct (W_{0}). The second sample is prepared at an angle of 75° (W_{75}) by using PVD method. In the deposition process, the thickness and the rate of deposition are controlled by digital thickness display monitor. To keep the

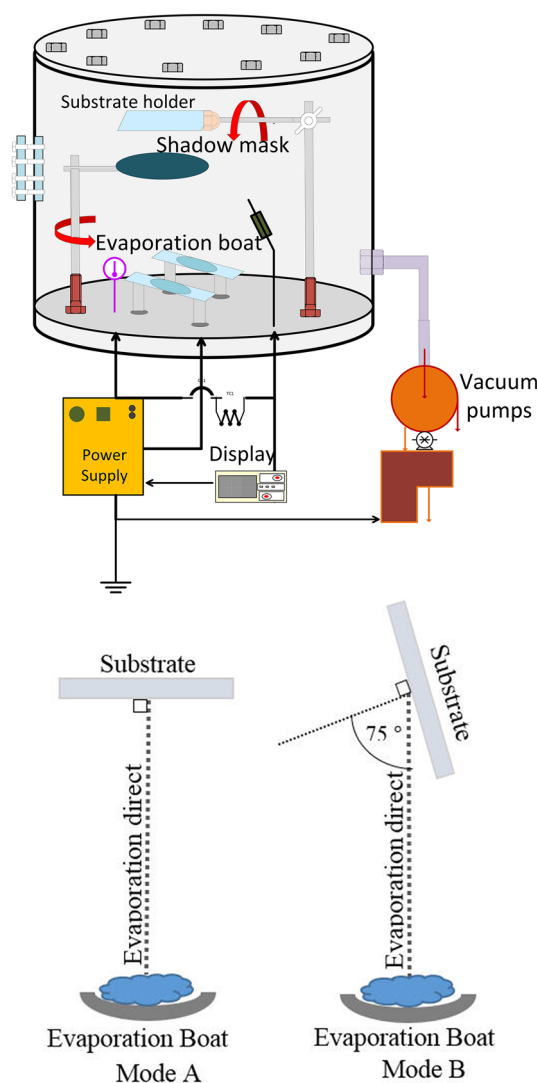


Fig. 1 Different modes of substrate holder in deposition process by physical vapor deposition

same deposition parameters in deposition process, the rate of deposition is fixed at 0.2 Å/s by increasing the step by step of current for each of samples (Fig. 2). In the next process, Ag nanoparticles as a dopant are decorated by PVD method at the same angle 0° for two samples (WAg₀ and WAg₇₅). In this process, deposition process is continued with deposition rate of 0.1 Å/s for 2 min. The annealing process to crevasse the Ag nanoparticles is applied for 1 min and at 400 °C.

3 Results and discussion

3.1 Optical properties

In order to describe the photo-absorption behavior and optical band gap of the samples, the UV–Vis absorption spectra are recorded. Figure 3 shows the absorption spectra of tungsten oxide, WAg₀ and WAg₇₅ samples in the range of 300–800 nm. It can be seen that amount of absorption for WAg₀ sample at the range of 350–450 nm and 650–800 nm is higher than WAg₇₅ sample. Conversely, the amount of absorption for WAg₀ sample at the middle wavelengths (450–650 nm) is smaller than WAg₇₅ sample. On the other hand, absorption of tungsten oxide thin film shows the lowest amount compared to composite samples. This is because the contribution of silver particles absorption is also found in composite samples. In addition, the band gap values (Fig. 4) are calculated using Eq. 2:

$$\alpha h\nu = A(h\nu - E_g)^n \quad (2)$$

where A is a constant which depends on the electronic transition probability, $h\nu$ denotes photon energy, E_g is the optical energy gap of the material, and n is the power which

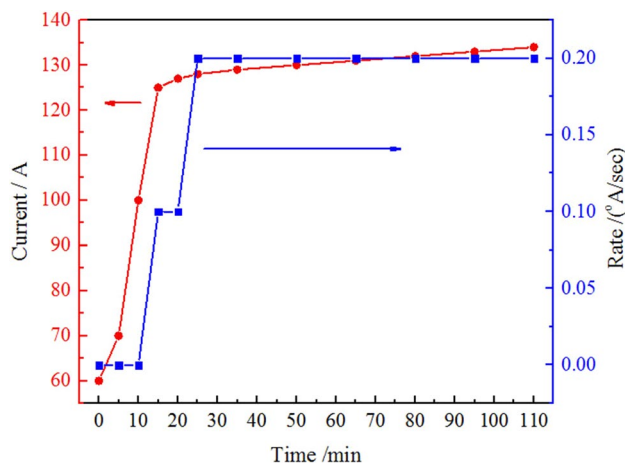


Fig. 2 The curves of current and deposition rate vs. time in deposition process. (Color figure online)

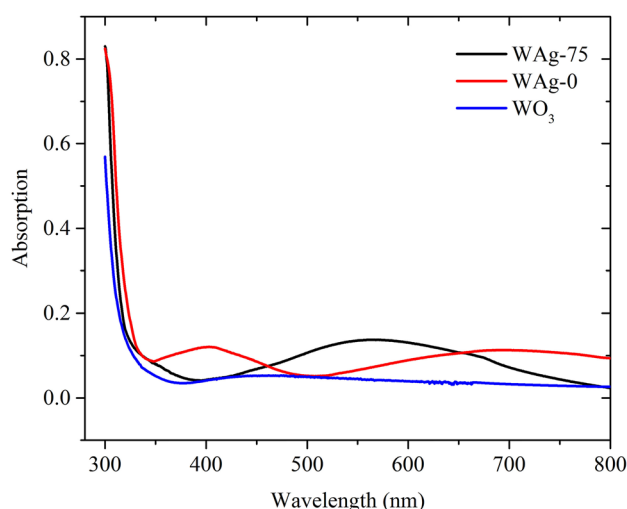


Fig. 3 Absorption curves of WO₃ (blue curve), WAg₀ sample (red curve) and WAg₇₅ sample (black curve) vs. wavelength. (Color figure online)

characterizes the transition process, where $n = 1/2$ and $3/2$ for direct allowed and forbidden transitions, respectively, and $n = 2$ and 3 for indirect allowed and forbidden transitions, respectively [19]. For WAg₀, WAg₇₅ and tungsten oxide samples (Fig. 4), we observe band gaps at 3.78, 3.85 and 3.89 eV, respectively. It can be seen that with increasing the dopant amount of nanoparticles (Ag) to semiconductor material (WO₃), the band gap is decreased. Additionally, WAg₇₅ sample shows a lower band gap than WAg₀ sample. Therefore, this suggests that WAg₇₅ sample has had a better condition to form uniform composite.

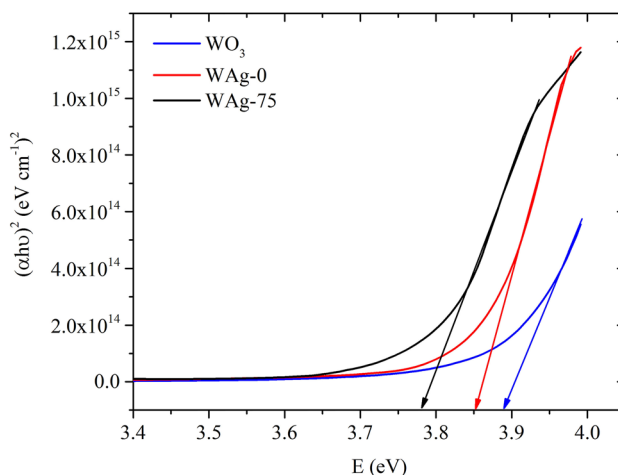


Fig. 4 The Tauc plots that shows photon energy dependence of $(\alpha h\nu)^2$ for WO₃ (blue curve), WAg₀ sample (red curve) and WAg₇₅ sample (black curve)

3.2 Morphology studies

The morphologies of the WAg_{0} and WAg_{75} thin films are determined by using FESEM and AFM techniques. Figure 5a, b show the FESEM images corresponding to WAg_{0} thin film. As can be seen, these pictures are consisted of a cleft surface that cracks are very narrow and small. On the other hand, Fig. 5d, e show the FESEM images corresponding to WAg_{75} thin film that its surface porosity is very deep and broad compared to the WAg_{0} sample. The surface of WAg_{75} thin film not only provides suitable surface to penetrate Ag nanoparticles into depth of surface, but also increases the effective surface in contact with the electrolyte and subsequently enhances the EC performance. Figure 5c, f show the EDX of WAg_{0} and WAg_{75} samples that confirm the presence of fundamental elements for each sample. In Fig. 5c, f, three fundamental elements of WO_3 -Ag thin films can be observed. The weight and atomic percentages of elements in structures of the thin films are reported in Table 1. Figure 6 shows the AFM images of WAg_{0} and WAg_{75} thin films for scanning a square area $3\ \mu\text{m} \times 3\ \mu\text{m}$. In Fig. 6a can be seen that the morphology of the WAg_{0} surface has an approximate

Table 1 The detailed structures of the WAg_{0} and WAg_{75} thin films

Sample	Element	Wt%	At. %
WAg_{0}	O	23.42	77.44
	W	73.99	21.29
	Ag	2.59	1.27
WAg_{75}	O	24.21	78.14
	W	72.89	20.47
	Ag	2.9	1.39

roughness about 14 nm and Fig. 6b shows that surface morphology of the WAg_{75} thin film has roughness about 20 nm. The depth histograms associated with AFM images of the samples obtained at two different deposition direct are shown in the corresponding Fig. 6a, b. It enables to observe the density of the distribution of the data points on the surface. The vertical axis of the histograms is graduated in depths: the horizontal axis is graduated in percentage of the whole population. There is, however, an increase in the surface roughness with increasing the angle of deposition direct, with root mean squared roughness of 20 nm compared to 14 nm for these samples.

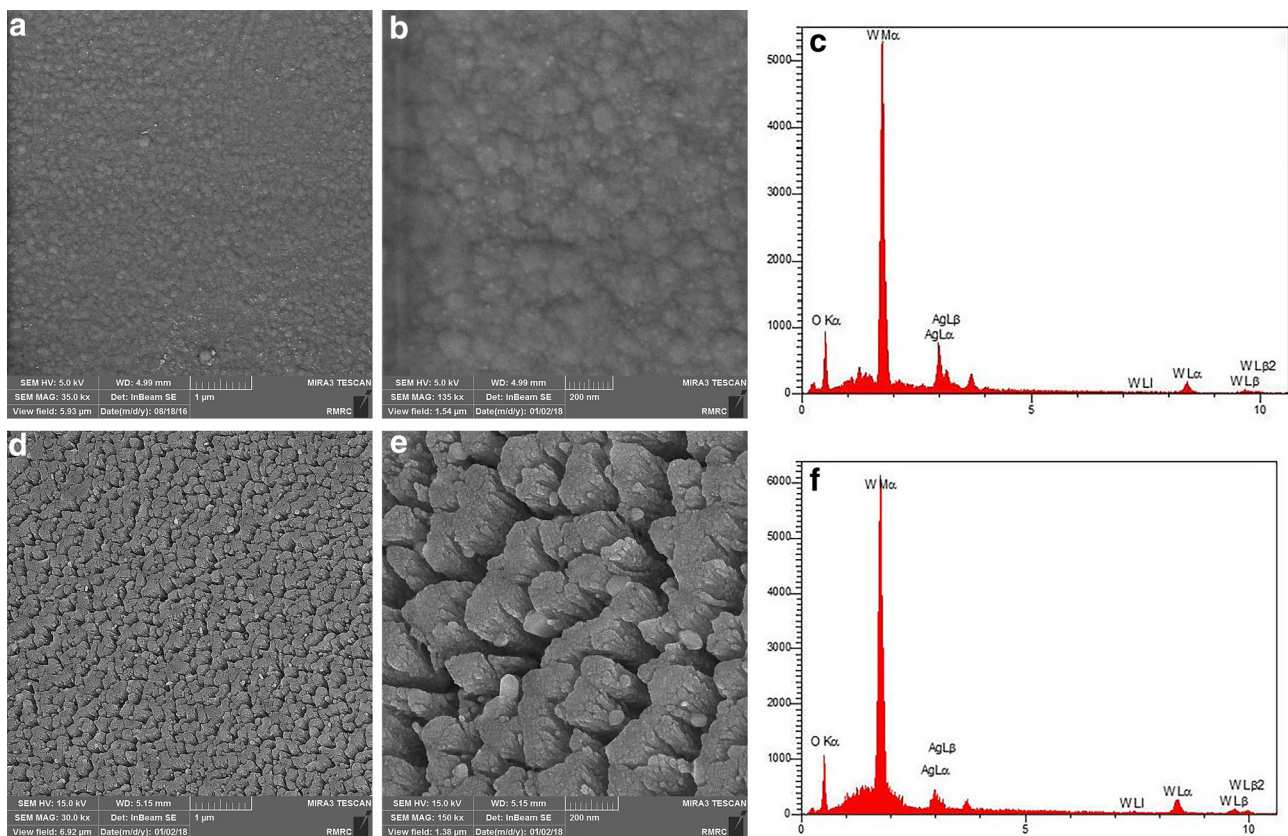
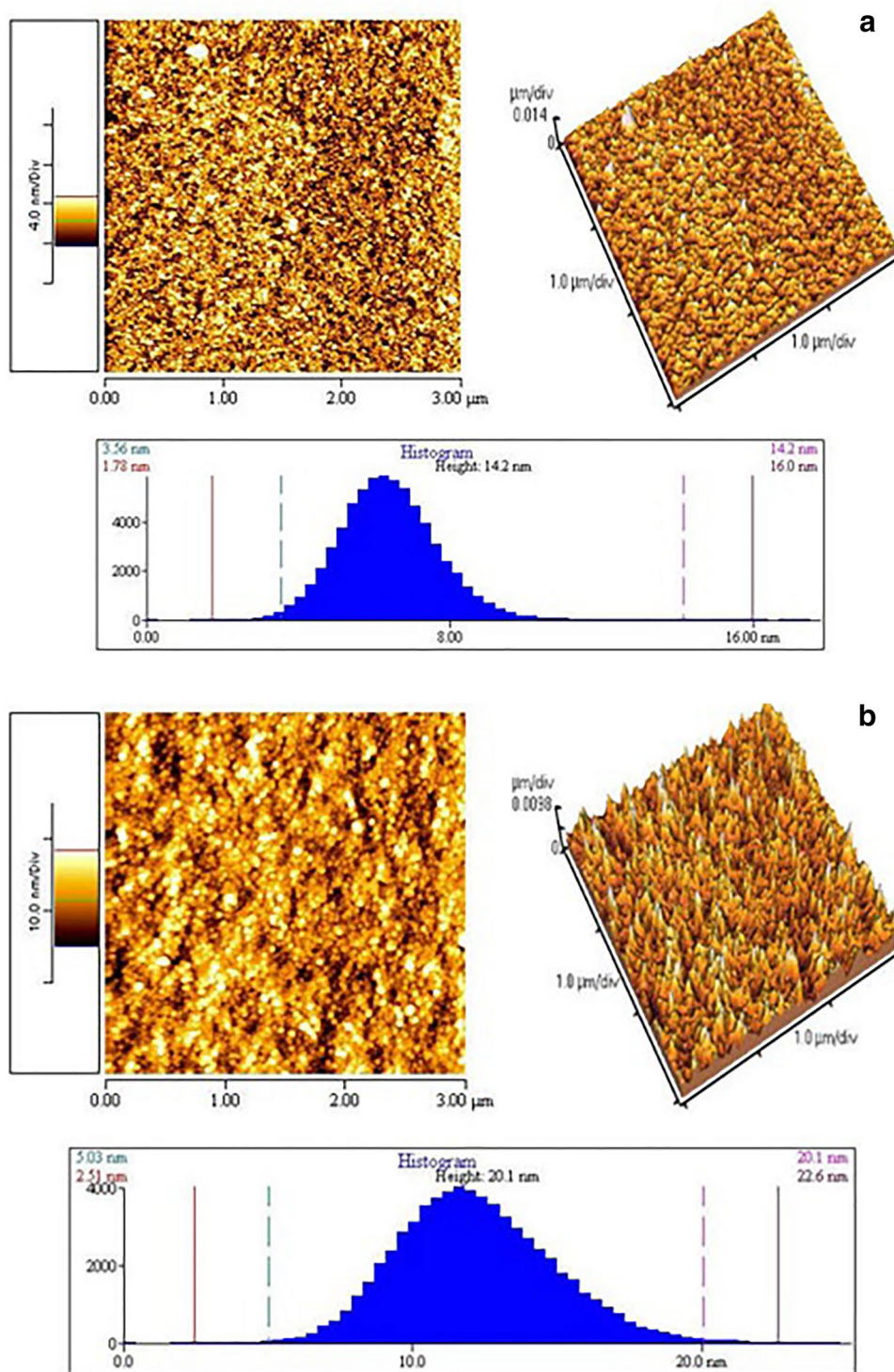


Fig. 5 FESEM images and EDX spectra of **a–c** WAg_{0} sample and **d–f** WAg_{75} sample

Fig. 6 AFM images of **a** WAg_{0} sample and **b** WAg_{75} sample. Scan size is $3\ \mu\text{m} \times 3\ \mu\text{m}$



3.3 XRD and X-ray photoelectron spectroscopy studies

In order to study the purity and crystal structure of samples, we use the XRD analyze and the results can be seen in Fig. 7. XRD measurements show that both WAg_{0} and WAg_{75} films are amorphous. But three common diffraction

peaks (for two samples) are observed at $2\theta = 38.3^\circ, 44.3^\circ, 64.4^\circ$ which correspond to (111), (200), (220) planes of metallic silver respectively (JCPDS ICDD04-0783). On the other hand, two special diffraction peaks are observed in WAg_{0} sample, which correlated to silver oxide (JCPDS ICDD74-1743).

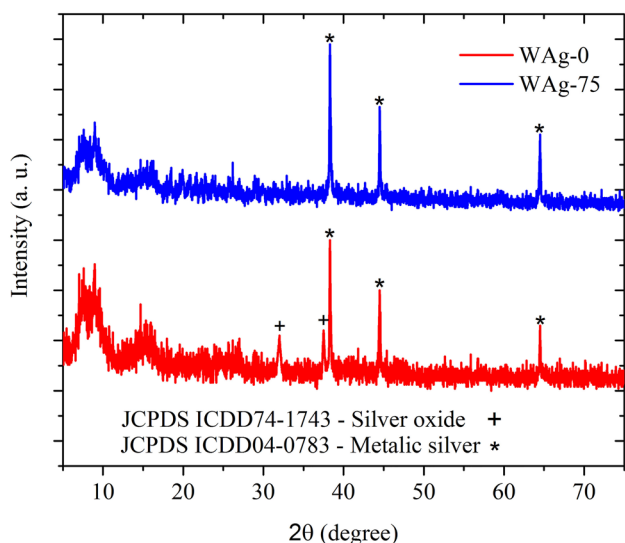


Fig. 7 XRD pattern of silver–tungsten oxide composite films. The blue and red spectra are correlated to WAg₇₅ and WAg₀ samples. (Color figure online)

In order to study the stoichiometry of composite samples after post annealing process, we have done X-ray photoelectron spectroscopy (XPS) for samples and XPS spectra showed different results. Figure 8 shows the XPS results including the survey, WO₃ and Ag spectra of WAg₀ and WAg₇₅ samples and Fig. 8a shows that all deposited films are contamination free. As can be seen, Fig. 8b shows high resolution scans of W4f peaks for films deposited at different states. The peak located at approximately 41.7 eV is attributed to W5p_{3/2} while the other doublet peaks located at 35.7 and 37.7 eV are attributed to W4f_{7/2} and W4f_{5/2} (the peaks have a full width at half-maximum of 2.0 eV and an intensity ratio of 0.75) and the tungsten oxide films do not exhibit any sub-stoichiometry [20, 21]. Figure 8c shows high resolution scans of Ag3d peaks for samples. After annealing process, the Ag3d_{5/2} and Ag3d_{3/2} doublet peaks are located at 367.4 and 373.5 eV that are attributed to AgO particles for WAg₀ sample, while these peaks are located at 386.3 and 374.4 eV are denoted to Ag particles for WAg₇₅ sample [22, 23]. Then the surface morphology difference is caused that the silver

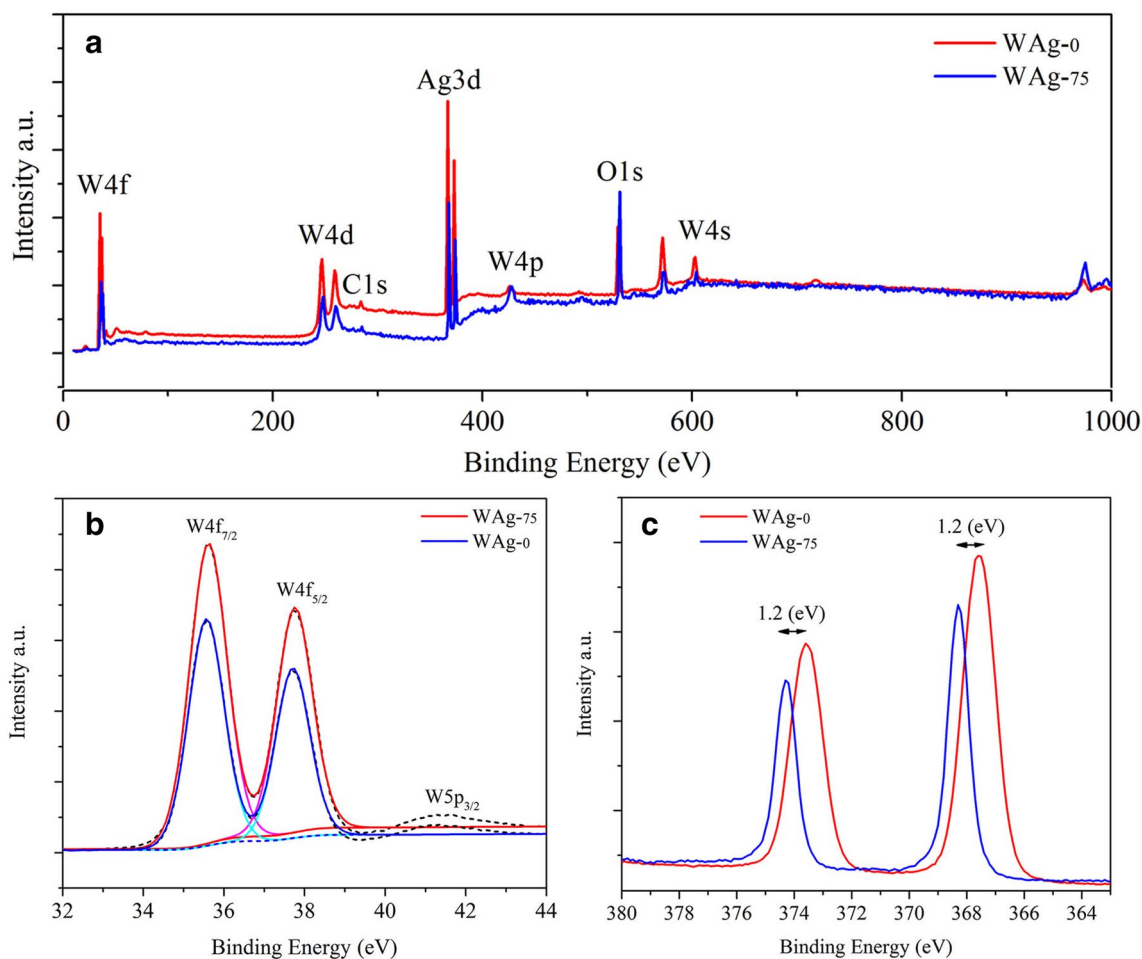


Fig. 8 XPS spectra of WAg₀ and WAg₇₅ samples. **a** Survey, **b** high resolution XPS scans of W4f peaks and **c** high resolution XPS scans of Ag3d peaks

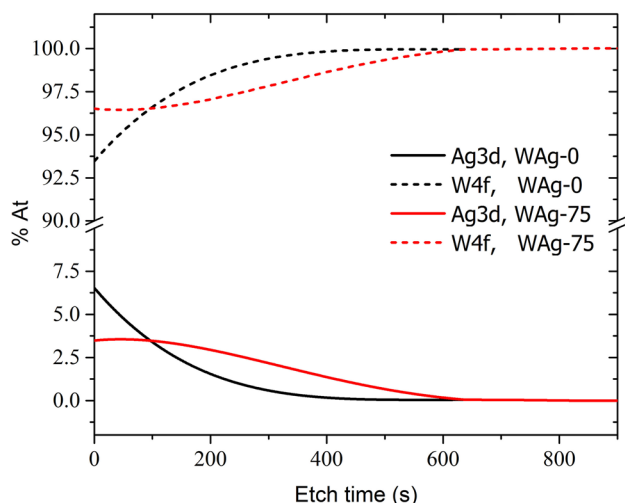


Fig. 9 XPS depth profile of samples for W4f and Ag3d peaks

particles diffused into the WO_3 layer of $\text{WAg}_{.75}$ sample and are prevented from oxidation in air.

In order to investigate the depth of silver penetration into tungsten oxide films, we use XPS depth profile analyze for samples and the result are shown in Fig. 9. These curves show the atomic percentages of tungsten and silver due to W4f and Ag3d peaks. The Ag atomic percentage on the surface of film correlated to $\text{WAg}_{.0}$ sample is higher than $\text{WAg}_{.75}$ sample. It shows that the difference in surface leads to this result. In the other words, more porosity of the tungsten oxide surface of in the $\text{WAg}_{.75}$ sample has contributed to the deeper penetration of silver particles. In addition, the penetration depth of silver particles into $\text{WAg}_{.0}$ sample indicates that the post annealing process is associated in metal particles penetration process, although it is trifle compared to influence of surface porosity. The presence of silver particles in depth of $\text{WAg}_{.75}$ sample, contrary to $\text{WAg}_{.0}$ sample, leads to enhance the EC performance through the silver SPR.

3.4 CV studies

Figure 10 exhibits the CV curves of $\text{WAg}_{.0}$ and $\text{WAg}_{.75}$ samples in 0.5 M $\text{LiClO}_4\text{-PC}$ solution in the potential region from -1.0 to $+1.0$ V (vs. Ag/AgCl) at scan rate of 50 mV/s. These curves compare the influence of surface morphology of samples. As can be seen, $\text{WAg}_{.0}$ sample exhibits the oxidation broad peak at -0.4 V and the reduction broad peak due to the intercalation process of Li^+ into and the deintercalation of Li^+ out from the $\text{WAg}_{.0}$ thin film. On the other hand, $\text{WAg}_{.75}$ sample shows the oxidation broad peak at -0.1 V that is happened after peak of $\text{WAg}_{.0}$ sample and has an excellent conductivity at positive and negative potentials. It is because of that the recorded current is due to the Li^+ ion intercalation/extraction according to the surface porosity,

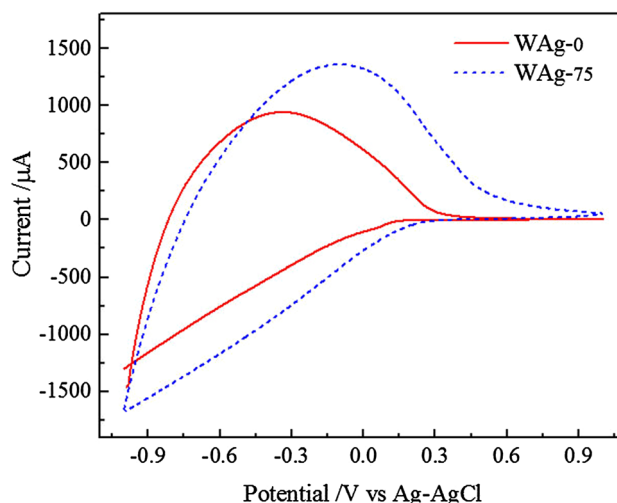


Fig. 10 Cyclic voltammogram of $\text{WAg}_{.0}$ sample (red line) and $\text{WAg}_{.75}$ sample (blue line) in a 0.5 M solution of $\text{LiClO}_4\text{-PC}$. (Color figure online)

which increases the contact surface with electrolyte containing Li^+ ions. In other words, the entry and exit of more ions into the host network structure will enhance electrochemical performance. This indicate that the $\text{WAg}_{.75}$ sample has higher electrochemical activity associated with more area inside of CV curve.

3.5 EC properties

The EC properties, such as contrast change, response time and coloration efficiency (CE) of the $\text{WAg}_{.0}$ and $\text{WAg}_{.75}$ thin films are reported. When $\text{WAg}_{.0}$ and $\text{WAg}_{.75}$ thin films are cathodically colored, they change their transparent state and transform to uniform dark blue color. Mutually, when these dark blue thin films are anodically bleached, they recapture their transparent state. This reversible process can be achieved at different applied DC voltage from -1.0 to $+1.0$ V and vice versa. The visible transmittance spectra of the $\text{WAg}_{.0}$ and $\text{WAg}_{.75}$ thin films under different DC voltage are recorded in Fig. 11. The maximum value of the optical transmittance of the $\text{WAg}_{.0}$ thin film in bleached state is 82.18% at 632.8 nm while the minimum value of the optical transmittance in colored state is 45.15% in the same wavelength. Hence, the contrast change ($\Delta T = T_b - T_c$ where T_b represents the transmittance in the bleached state and T_c represents the transmittance in the colored state) for $\text{WAg}_{.0}$ thin film is equal to 37.03% at 632.8 nm. The visible transmittance of the $\text{WAg}_{.75}$ thin film decreases from 83.68 to 43.09% at 632.8 nm when the potential is changed in steps between $+1.0$ and -1.0 V. Therefore, the maximum difference of transmittance for this thin film is equal to 40.59% at 632.8 nm that is higher than the

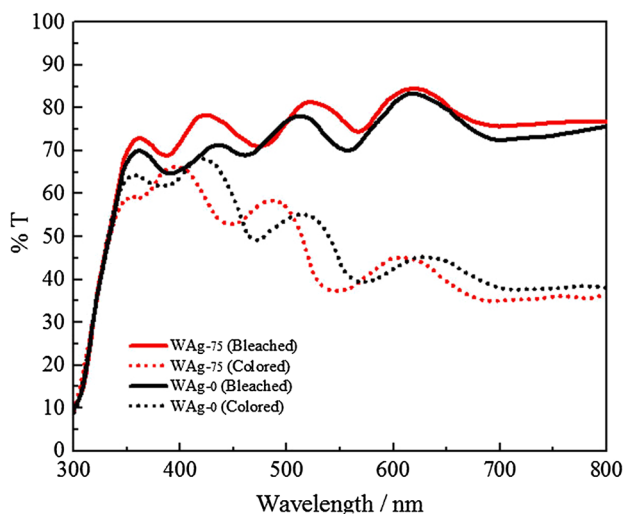


Fig. 11 Visible transmittance spectra of WAg₀ sample and WAg₇₅ sample under different potentials from −1.0 to +1.0 V

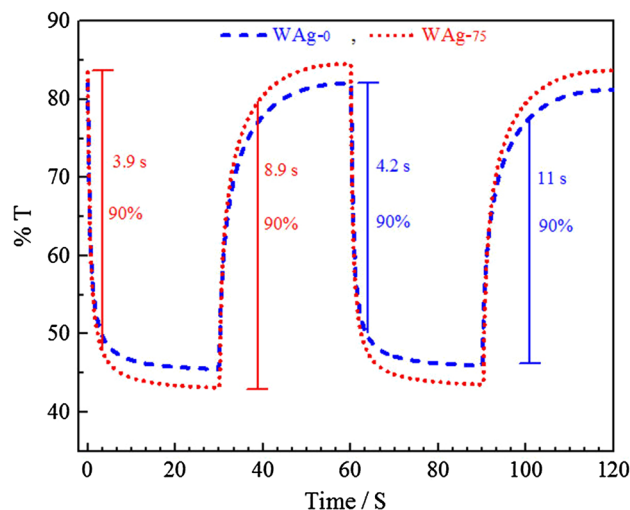


Fig. 12 Electrochromic responses at 632.8 nm for WAg₀ sample (−1.0 to +1.0 V) and WAg₇₅ sample (−1.0 to +1.0 V) in 0.5 M LiClO₄-PC electrolyte

maximum difference of transmittance for WAg₀ thin film. These values are presented in Table 2, briefly. The collective oscillations of the free conduction band electrons in Ag nanoparticles by incident light in the visible light cause photonic absorption in red region, rendering blue color to the silver particles [24]. Thus, both EC and SPR are going together and subsequently boost the coloration process.

The coloration switching response is other effective parameter that must be considered in the fabrication of ECDs. The response time is introduced as the required time for 90% change in the full transmittance modulation at 632.8 nm. In Fig. 12, we have shown the switching curves at 632.8 nm for WAg₀ and WAg₇₅ thin films in 0.5 M LiClO₄-PC electrolyte. The DC voltage step for the WAg₇₅ thin film is applied from −0.1 to +1.0 V and subsequently, the response time for bleached and colored states is evaluated as 8.9 and 3.9 s, which are faster than those of the WAg₀ thin film (11 and 4.2 s). The penetration depth of Ag nanoparticles can be caused charge transfer between the WO₃ and Ag nanoparticles the surface arising from plasmon resonance effect [18, 25]. The charge transfer process due to SPR decreases the time switching for composite thin films. Deeper penetration of Ag particles into WO₃ film in WAg₇₅ sample compared to WAg₀ sample is decreased the time switching from 11 to 8.9 s.

In Fig. 13, we have also compared the current densities of WAg₀ and WAg₇₅ thin films at different sequential switching from +1.0 V to −1.0 and from −1.0 to +1.0 V. In this process, the total charge inserted (or extracted) through the electrodes can be evaluated using the Eq. 3 [26]:

$$Q = \int i dt \tag{3}$$

Hence, as we observed, the interchanged charge in WAg₇₅ thin film is less than WAg₀ thin film.

Another measurable parameter in EC process is CE that is calculated from Eqs. 4 and 5 [27, 28]:

$$CE = \Delta OD / (Q/A) \tag{4}$$

$$\Delta OD(\lambda) = \log \frac{T_b}{T_c} \tag{5}$$

where Q is the injected electronic charge per unit area, T_c and T_b are transmission of thin films at λ=632.8 nm in colored and bleached states, respectively. Figure 14 shows the plot of ΔOD at 632.8 nm vs. the charge density at coloration DC voltage −1.0 V for WAg₀ and WAg₇₅ thin films. The CE values of samples are calculated to be 71.9 cm² C^{−1} for WAg₀ and 90.2 cm² C^{−1} for WAg₇₅ thin films.

Table 2 Electrochromic properties of WAg₀ and WAg₇₅ thin film in 0.5 M solution LiClO₄-PC at 632.8 nm

Sample	DC voltage steps (V)	T _c (%)	T _b (%)	ΔT (%)	CE (cm ² C ^{−1})	τ _C (s)	τ _B (s)	Γ(λ) (cm ² C ^{−1} s ^{−1})
WAg ₀	+1.0 to −1.0	45.15	82.18	37.03	71.9	4.2	11	9.46
WAg ₇₅	+1.0 to −1.0	43.09	83.68	40.59	90.2	3.9	8.9	14.09

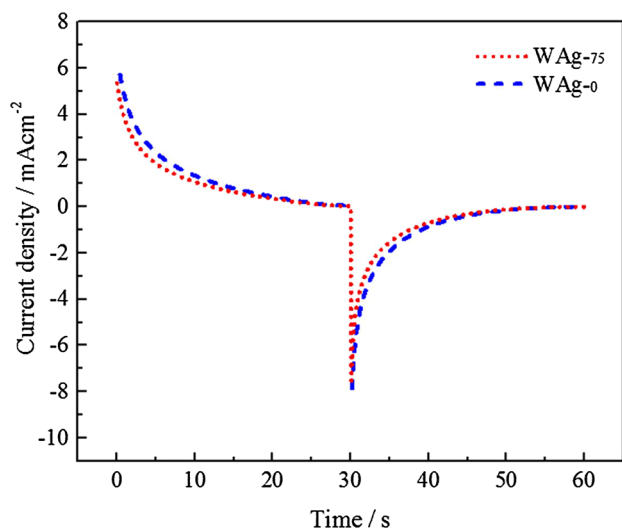


Fig. 13 The current curves vs. time for WAg₀ sample (−1.0 to +1.0 V) and WAg₇₅ sample (−1.0 to +1.0 V) in 0.5 M LiClO₄-PC electrolyte

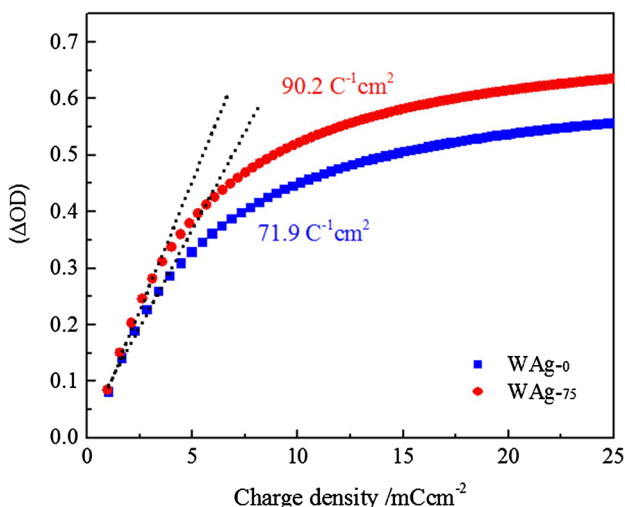


Fig. 14 Variation of the in situ optical density (OD) vs. charge density for WAg₀ and WAg₇₅ samples

In order to present the overall EC performances of the thin films, the quality factor $\Gamma(\lambda)$ can be evaluated by Eq. 6 [29]:

$$\Gamma(\lambda) = \frac{CE}{\tau}, \quad \tau = \frac{\tau_c + \tau_b}{2} \quad (6)$$

where τ is the mean value of the coloring and bleaching time. The overall EC performances of the WAg₀ and WAg₇₅ thin films are 9.46 and 14.09 cm² C⁻¹ s⁻¹, respectively, indicating that the EC performance of the WAg₇₅ thin film was better than that of the WAg₀ thin film.

4 Conclusions

The WO₃ thin films are deposited on FTO-coated glass substrates by PVD method at two different modes. The orientable substrate holder is used to deposit the porous surface of WO₃ thin film by PVD. The Ag nanoparticles are decorated on WO₃ thin films with different surface morphologies by PVD method and annealed in vacuum at 400 °C for 1 min. The post annealing process is used to penetrate Ag nanoparticles into WO₃ layers. The obtained results from XPS depth profiling measurement show that deeper penetrate of Ag particles achieved for WAg₇₅ sample due to more porous surface compared to WAg₀ sample. Thus, the different WO₃-Ag nanocomposite thin films are prepared and then studied to evaluate the influence of surface morphology on EC properties. The WAg₇₅ sample has been upgraded some of the advantages and properties to use in ECDs based on silver SPR and different surface morphology. First, the change of transmittance percentage of WAg₇₅ sample at 632.8 nm has been increased to 40.59% at DC voltage steps −1.0 to +1.0 V in 0.5 M LiClO₄-PC solution. Second, the response time of WO₃-Ag thin film for bleached states has been decreased from 11 to 8.9 s and for colored states decreased from 4.2 to 3.9 s at same DC voltage steps. Third, the CE of WAg₇₅ sample at 632.8 nm has been increased to 90.2 cm² C⁻¹.

References

1. S. Vidya, S. Solomon, J.K. Thomas, Synthesis and characterisation of MoO₃ and WO₃ nanorods for low temperature co-fired ceramic and optical applications. *J. Mater. Sci.: Mater. Electron.* **26**(5), 3243–3255 (2015)
2. Y.E. Firat, A. Peksoz, Electrochemical synthesis of polyaniline/inorganic salt binary nanofiber thin films for electrochromic applications. *J. Mater. Sci.: Mater. Electron.* **28**(4), 3515–3522 (2017)
3. M. Roeder, A.B. Beleke, U. Guntow, J. Buensow, A. Guerfi, U. Posset, H. Lorrmann, K. Zaghbi, G. Sextl, Li₄Ti₅O₁₂ and LiMn₂O₄ thin-film electrodes on transparent conducting oxides for all-solid-state and electrochromic applications. *J. Power Sources* **301**, 35–40 (2016)
4. H. Najafi-Ashtiani, A. Bahari, S. Ghasemi, A dual electrochromic film based on nanocomposite of copolymer and WO₃ nanoparticles: enhanced electrochromic coloration efficiency and switching response. *J. Electroanal. Chem.* **774**, 14–21 (2016)
5. X. Wu, W. Zhang, Q. Wang, Y. Wang, H. Yan, W. Chen, Hydrogen bonding of graphene/polyaniline composites film for solid electrochromic devices. *Synth. Met.* **212**, 1–11 (2016)
6. G.Y. Sun, X. Cao, H. Zhou, S. Bao, P. Jin, A novel multifunctional thermo-chromic structure with skin comfort design for smart window application. *Sol. Energy Mater. Sol. Cells* **159**, 553–559 (2017)
7. M. Hočevar, U.O. Krašovec, Cubic WO₃ stabilized by inclusion of Ti: applicable in photochromic glazing. *Sol. Energy Mater. Sol. Cells* **154**, 57–64 (2016)

8. R. Lakshmanan, P.P. Raja, N.C. Shivaprakash, S. Sindhu, Fabrication of fast switching electrochromic window based on poly (3, 4-(2, 2-dimethylpropylenedioxy) thiophene) thin film. *J. Mater. Sci.: Mater. Electron.* **27**(6), 6035–6042 (2016)
9. S. Oukassi, C. Giroud-Garampon, C. Dubarry, C. Ducros, R. Salot, All inorganic thin film electrochromic device using LiPON as the ion conductor. *Sol. Energy Mater. Sol. Cells* **145**, 2–7 (2016)
10. S.Y. Kao, C.W. Kung, H.W. Chen, C.W. Hu, K.C. Ho, An electrochromic device based on all-in-one polymer gel through in-situ thermal polymerization. *Sol. Energy Mater. Sol. Cells* **145**, 61–68 (2016)
11. S. Zhang, R. Fu, Y. Gu, L. Dong, J. Li, S. Chen, Preparation of nanocellulose-based polyaniline composite film and its application in electrochromic device. *J. Mater. Sci.: Mater. Electron.* **28**(14), 10158–10165 (2017)
12. H. Najafi-Ashtiani, A. Bahari, S. Ghasemi, A dual electrochromic film based on nanocomposite of aniline and o-toluidine copolymer with tungsten oxide nanoparticles. *Org. Electron.* **37**, 213–221 (2016)
13. A.K. Chaudhari, V.B. Singh, Mechanical and physical properties of electrodeposited Ni-Fe, WO₃ doped nanocomposite. *Surf. Coat. Technol.* **307**, 683–692 (2016)
14. R. Mukherjee, P.P. Sahay, Effect of precursors on the microstructural, optical, electrical and electrochromic properties of WO₃ nanocrystalline thin films. *J. Mater. Sci.: Mater. Electron.* **26**(8), 6293–6305 (2015)
15. S.J. Lu, C. Wang, H. Wang, J.B. Liu, H. Yan, Excellent electrochromic properties of tungsten oxide films with a mesoporous structure. *J. Mater. Sci.: Mater. Electron.* **1–7** (2017)
16. L. Wang, Y.R. Hu, G.Q. Li, W. Xie, Formation and transmittance property of WO₃ films deposited by mid-frequency dual-target magnetron sputtering. *Surf. Coat. Technol.* **201**(9), 5063–5067 (2007)
17. K.W. Park, Electrochromic properties of Au-WO₃ nanocomposite thin-film electrode. *Electrochim. Acta* **50**, 4690–4693 (2005)
18. M.A. Gondal, M.A. Suliman, M.A. Dastageer, G.K. Chuah, C. Basheer, D. Yang, A. Suwaiyan, Visible light photocatalytic degradation of herbicide (Atrazine) using surface plasmon resonance induced in mesoporous Ag-WO₃/SBA-15 composite. *J. Mol. Catal. A* **425**, 208–216 (2016)
19. H. Najafi-Ashtiani, A. Bahari, Optical, structural and electrochromic behavior studies on nanocomposite thin film of aniline, o-toluidine and WO₃. *Opt. Mater.* **58**, 210–218 (2016)
20. Y. Baek, K. Yong, Controlled growth and characterization of tungsten oxide nanowires using thermal evaporation of WO₃ powder. *J. Phys. Chem. C* **111**(3), 1213–1218 (2007)
21. M. Nazari, F. Golestani-Fard, R. Bayati, B. Eftekhari-Yekta, Enhanced photocatalytic activity in anodized WO₃-loaded TiO₂ nanotubes. *Superlattices Microstruct.* **80**, 91–101 (2015)
22. M. Murugavelu, B. Karthikeyan, Study of Ag-Pd bimetallic nanoparticles modified glassy carbon electrode for detection of L-cysteine. *Superlattices Microstruct.* **75**, 916–926 (2014)
23. M. Biemann, P. Schwaller, P. Ruffieux, O. Gröning, L. Schlapbach, P. Gröning, AgO investigated by photoelectron spectroscopy: evidence for mixed valence. *Phys. Rev. B* **65**(23), 235431 (2002)
24. R.R. Kharade, S.S. Mali, S.P. Patil, K.R. Patil, M.G. Gang, P.S. Patil, J.H. Kim, P.N. Bhosale, Enhanced electrochromic coloration in Ag nanoparticle decorated WO₃ thin films. *Electrochim. Acta* **102**, 358–368 (2013)
25. Z. Liu, J. Wu, J. Zhang, Quantum dots and plasmonic Ag decorated WO₃ nanorod photoanodes with enhanced photoelectrochemical performances. *Int. J. Hydrogen Energy* **41**(45), 20529–20535 (2016)
26. N. Naseri, R. Azimirad, O. Akhavan, A.Z. Moshfegh, Improved electrochromical properties of sol-gel WO₃ thin films by doping gold nanocrystals. *Thin Solid Films* **518**, 2250–2257 (2010)
27. O.D. Coşkun, S. Demirel, G. Atak, The effects of heat treatment on optical, structural, electrochromic and bonding properties of Nb₂O₅ thin films. *J. Alloy. Compd.* **648**, 994–1004 (2015)
28. S. Hoseinzadeh, R. Ghasemiasl, A. Bahari, A.H. Ramezani, The injection of Ag nanoparticles on surface of WO₃ thin film: enhanced electrochromic coloration efficiency and switching response. *J. Mater. Sci.: Mater. Electron.* **28**(19), 14855–14863 (2017)
29. H. Li, Y. Lv, X. Zhang, X. Wang, X. Liu, High-performance ITO-free electrochromic films based on bi-functional stacked WO₃/Ag/WO₃ structures. *Sol. Energy Mater. Sol. Cells* **136**, 86–91 (2015)